JOURNAL OF MAGNETIC RESONANCE, Series B **113,** 151–159 (1996)
ARTICLE NO. 0168

Dependence of Saturation-Transfer EPR Intensities on Spin–Lattice Relaxation

T. PÁLI,* V. A. LIVSHITS,† AND D. MARSH

Abteilung Spektroskopie, Max-Planck-Institut für biophysikalische Chemie, Am Fassberg, D-37077 Göttingen, Germany

Received June 3, 1996

The intensities of saturation-transfer EPR (ST-EPR) spectra from nitroxyl spin labels have proved a sensitive means for studying slow exchange processes (both Heisenberg spin exchange and physical/chemical exchange) and weak interactions with paramagnetic ions, via the dependence on the effective spin–lattice relaxation rate (D. Marsh, *Appl. Magn. Reson.* **3, 53, 1992). The dependences of the second-harmonic EPR absorption intensities detected in phase quadrature with the field modulation (V_2' display) on the microwave H_1 field, and on the effective relaxation times, were studied both theoretically and experimentally. Power-saturation curves and normalized integrated intensities (I_{ST}) of the V_2' spectra were determined as a function of the concentration of a spin-labeled phospholipid in lipid membranes and of the concentration of paramagnetic Ni^{2+} ions in the aqueous phase as a means of varying the effective relaxation times. The results were correlated with progressive-saturation measurements of the double-integrated intensities of the conventional EPR spectra. Intensities of the V_2' spectra were calculated from the Bloch equations incorporating the modulation and microwave fields (K. Halbach,** *Helv. Phys. Acta* **27, 259, 1954), and the results were fitted to the experimental data. The ST-EPR intensities depend approximately linearly on the effective T_1, but with a nonzero intercept. On the basis of the theoretical calculations and experimental correlations, relations between I_{ST} and T_1 are suggested that may improve precision in the application of this alternative form of ST-EPR spectroscopy to biological systems.**

INTRODUCTION

Saturation-transfer EPR (ST-EPR) is a nonlinear CW spectroscopy that has proved to be particularly effective for studying the slow rotational diffusion of spin-labeled biomolecules that takes place on the time scale of the spin–lattice relaxation (*1*). The transfer of saturation by rotational motion gives rise to characteristic changes in the lineshape of the anisotropic nonlinear spectra that may be used to determine the rotational correlation time. There is, however, another class of slow dynamic processes, notably translational diffusion and exchange events, that do not depend on angular rotation but nonetheless contribute to the effective spin–lattice relaxation (*2*). Additionally, paramagnetic relaxation enhancements are expected to give rise to similar effects (*3*). All such processes are expected to have comparatively little influence on the spectral lineshapes but nevertheless affect the overall intensity of the ST-EPR spectrum (*4*). This alternative form of ST-EPR spectroscopy is less well-developed than the standard methods for studying slow rotational diffusion, but currently shows considerable potential (*2, 3*). Examples of applications at present include the study of slow translational diffusion (*4–6*), of slow molecular exchange, e.g., at the interface of integral membrane proteins (*7*), of membrane domain formation (*8*), and of dipolar relaxation by paramagnetic ions (*9*).

So far, this latter use of ST-EPR intensities to determine spin–lattice relaxation enhancements has relied principally on experimental correlations, for instance, a predictable dependence on spin-label concentration (*4, 5*) or on the concentration of paramagnetic ions (*9*). To assist in the further application of this newer nonlinear EPR method, it is therefore desirable to compare the results with theoretical predictions and with independent measurements that are sensitive to the spin–lattice relaxation. In the present work we have carried out such studies. The dependence of the ST-EPR intensities on the microwave field intensity and on the effective relaxation times obtained from progressive-saturation experiments has been investigated. The results have been fitted to theoretical simulations derived from solution of the Bloch equations that explicitly contain the microwave and Zeeman modulation fields. In this way, values have been obtained for the effective relaxation times and calibrations established

* Permanent address: Institute of Biophysics, Biological Research Center, H-6701 Szeged, Hungary.

† Permanent address: Institute of Chemical Physics, Russian Academy of Sciences, 117977, Moscow, Russian Federation.

1064-1866/96 $18.00

from which spin–lattice relaxation enhancements may be deduced from the measured ST-EPR intensities.

MATERIALS AND METHODS

Dipalmitoyl phosphatidylcholine (DPPC) was from Fluka (Buchs, Switzerland). Phosphatidylcholine spin-labeled on the 5 C-atom position of the *sn*-2 chain (5-PCSL) was synthesized as described in Ref. (*10*). DPPC and 5-PCSL were codissolved at the desired relative concentration (0.07–12 mol% 5-PCSL) in chloroform/methanol (2/1, v/v) and the solvent was then evaporated under nitrogen. The dry lipid was kept under vacuum overnight and then dispersed in argon-saturated distilled water or $NiCl_2$ solutions (0–50 mM) by vortex mixing at a temperature above the gel-to-fluid bilayer phase transition. Aliquots of the lipid dispersions were loaded into 100 μl, 1 mm diameter glass capillaries flushed with argon and pelletted in a bench-top centrifuge. Excess supernatant was removed to obtain lipid pellets of 5 mm length, sealed under argon. This standardized sample configuration was used for all progressive saturation and ST-EPR measurements (*11*, *12*).

EPR spectra were recorded at a microwave frequency of 9 GHz on a Varian Century Line spectrometer equipped with nitrogen gas-flow temperature regulation. Sample capillaries were accommodated in a standard quartz EPR tube that contained light silicone oil for thermal stability. The entire sample chamber was sealed under argon. Temperature was measured with a fine-wire thermocouple located within the capillary in contact with the sample. Samples were centered in the microwave cavity and all spectra were recorded under critical coupling conditions. The root-mean-square microwave magnetic field at the sample was measured as described in Ref. (*11*) and corrections were made for the cavity Q as described in the same reference.

ST-EPR spectra were recorded in the second-harmonic absorption mode at a modulation frequency of 50 kHz with detection in phase quadrature at 100 kHz (V_2' display). The modulation field at the sample was 5 G p-p and the mean microwave field at the sample was 0.25 G (*11*, *12*). The modulation phase was set by the self-null method at a subsaturating microwave field intensity. Integrated intensities of the V_2' ST-EPR spectra were normalized to the double-integrated intensity of the conventional, first-harmonic in-phase absorption spectrum (V_1),

$$I_{ST} = \frac{\int V_2'(H)dH}{\iint V_1(H)d^2H}, \qquad [1]$$

as defined in Ref. (*13*). Progressive-saturation experiments were performed with the conventional in-phase first-harmonic absorption spectra (V_1 display) with a modulation frequency of 100 kHz and a modulation amplitude of 1.25 G p-p. The double-integrated intensity, $I(H_1)$, of the conventional V_1 EPR spectra with increasing microwave field H_1 was fitted with the expression (*14*)

$$I(H_1) = \frac{I_0(H_1)}{(1 + \gamma_e^2 H_1^2 T_1 T_2)^{1/2}}, \qquad [2]$$

where $I_0(H_1)$ is the double-integrated intensity that would be obtained in the absence of saturation, to yield the effective T_1T_2 product.

THEORY

The calculation of the EPR intensities detected in phase quadrature with the field modulation follows that of Halbach (*15*). The magnetic field intensity along the z direction is given by $H = H_0 + H_m \cos \omega_m t$, where H_0 is the static field, H_m is the amplitude of the field modulation, and ω_m is the modulation frequency. The normalized complex magnetizations u, v, and w in the x, y, and z directions, respectively, of the rotating frame are expanded in Fourier harmonics, n, of the modulation frequency,

$$u = \sum_{-\infty}^{\infty} u_n e^{-in\omega_m t} \qquad [3]$$

$$v = \sum_{-\infty}^{\infty} v_n e^{-in\omega_m t} \qquad [4]$$

$$w = \sum_{-\infty}^{\infty} w_n e^{-in\omega_m t}, \qquad [5]$$

where the Fourier coefficients v_n and u_n correspond to the absorption and dispersion signals, respectively, detected at a frequency $n\omega_m$ (*16*).

The Bloch equations expressed in a frame rotating at the angular frequency, ω, of the H_1 microwave field yield the following relations for the Fourier coefficients of Eqs. [3]–[5] (*15*),

$$u_n(1 - in\omega') + Dv_n + k(v_{n-1} + v_{n+1}) = 0 \qquad [6]$$

$$v_n(1 - in\omega') - Du_n - k(u_{n-1} + u_{n+1}) + hw_n = 0 \qquad [7]$$

$$w_n(a - in\omega') - hv_n = a\delta_{n,0}, \qquad [8]$$

where $\delta_{n,0} = 1$ for $n = 0$, and is otherwise zero. In Eqs. [6]–[8], frequencies are expressed in terms of the transverse relaxation time, T_2, and magnetic fields in terms of the linewidth, $\Delta H = 1/\gamma_e T_2$, i.e.,

$$\omega' = \omega_m T_2$$
$$D = (H_0 - \omega/\gamma_e)/\Delta H$$
$$h = H_1/\Delta H$$
$$k = H_m/2\Delta H, \qquad [9]$$

where γ_e is the gyromagnetic ratio of the electron, and $a = T_2/T_1$, with T_1 being the spin–lattice relaxation time. A solution for the Fourier coefficients is obtained by expanding in powers of the normalized field modulation amplitude, k,

$$u_n = \sum_{\nu=0}^{\infty} u_{n,\nu} k^\nu \qquad [10]$$

$$v_n = \sum_{\nu=0}^{\infty} v_{n,\nu} k^\nu, \qquad [11]$$

where ν is always positive, or zero.

On substitution of these relations in Eqs. [6]–[8], with elimination of w_n, the following relations are obtained for the coefficients $u_{n,\nu}$ and $v_{n,\nu}$:

$$u_{n,\nu}(1 - in\omega') + Dv_{n,\nu} + v_{n-1,\nu-1} + v_{n+1,\nu-1} = 0 \qquad [12]$$

$$v_{n,\nu}\left(1 - in\omega' + \frac{h^2}{a - in\omega'}\right) - Du_{n,\nu}$$

$$- u_{n-1,\nu-1} - u_{n+1,\nu-1} = -h\delta_{n,0}. \qquad [13]$$

From the structure of Eqs. [6]–[8] and of Eqs. [12] and [13], it follows that the first nonzero terms correspond to $\nu = |n|$ and higher terms must have the same parity as $|n|$ (*15*). To lowest order in the modulation amplitude (i.e., $\nu = n$), the Fourier coefficients therefore are given by the following recurrence relations,

$$u_{n,n} = \frac{-[1 - in\omega' + h^2/(a - in\omega')]v_{n-1,n-1} - Du_{n-1,n-1} + Dh\delta_{n,0}}{D^2 + (1 - in\omega')[1 - in\omega' + h^2/(a - in\omega')]} \qquad [14]$$

$$v_{n,n} = \frac{(1 - in\omega')u_{n-1,n-1} - Dv_{n-1,n-1} - h\delta_{n,0}}{D^2 + (1 - in\omega')[1 - in\omega' + h^2/(a - in\omega')]}, \qquad [15]$$

where for $n = 0$, the terms with indices $n - 1$ are zero.

The expressions for the zeroth harmonic ($n = 0$) yield the usual slow-passage solutions of the Bloch equations,

$$u_{0,0} = hD/(1 + D^2 + h^2/a) \qquad [16]$$

$$v_{0,0} = -h/(1 + D^2 + h^2/a), \qquad [17]$$

representing the dispersion and absorption signals, respectively. The coefficients for higher harmonics are obtained by successive applications of Eqs. [14] and [15]. To the lowest order in the modulation amplitude, the Fourier coefficients of the nth harmonic are then given by $u_n \approx u_{n,n}k^n$ and $v_n \approx v_{n,n}k^n$. The real and imaginary parts of $v_{n,n}$ and $u_{n,n}$ yield the absorption and dispersion signals that are in-phase and 90° out-of-phase, respectively, with respect to the field modulation. Thus the conventional in-phase EPR spectra and the first-harmonic dispersion and second-harmonic absorption ST-EPR spectra, for instance, are given by, respectively,

$$V_1 \approx k\ \mathrm{Re}(v_{1,1})$$
$$U_1' \approx k\ \mathrm{Im}(u_{1,1})$$
$$V_2' \approx k^2 \mathrm{Im}(v_{2,2}), \qquad [18]$$

where the notation of Ref. (*1*) is used. Based on the lowest terms in the expansions of Eqs. [10] and [11], these approximations are valid for low modulation amplitudes.

RESULTS AND DISCUSSION

H_1 dependence of ST-EPR spectra. Simulated second-harmonic absorption spectra in phase quadrature with respect to the field modulation are given in Fig. 1, for a single

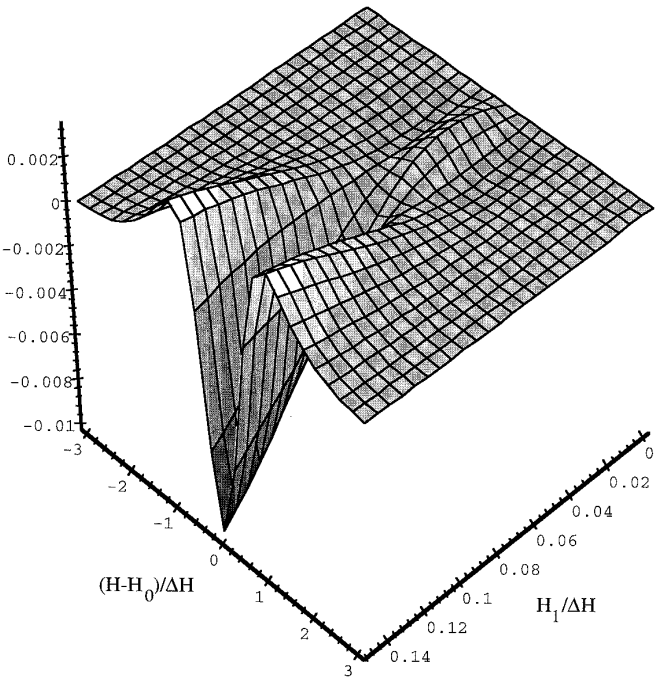

FIG. 1. Dependence of the simulated second-harmonic, 90° out-of-phase, absorption EPR spectra (V_2' display) for a single resonance line on the microwave magnetic field intensity, H_1. Simulations are for a Zeeman modulation frequency $\omega_m/2\pi$ = 50 kHz, spin–lattice relaxation time T_1 = 1 μs, and spin–spin relaxation time T_2 = 40 ns (ΔH = 1.4 G).

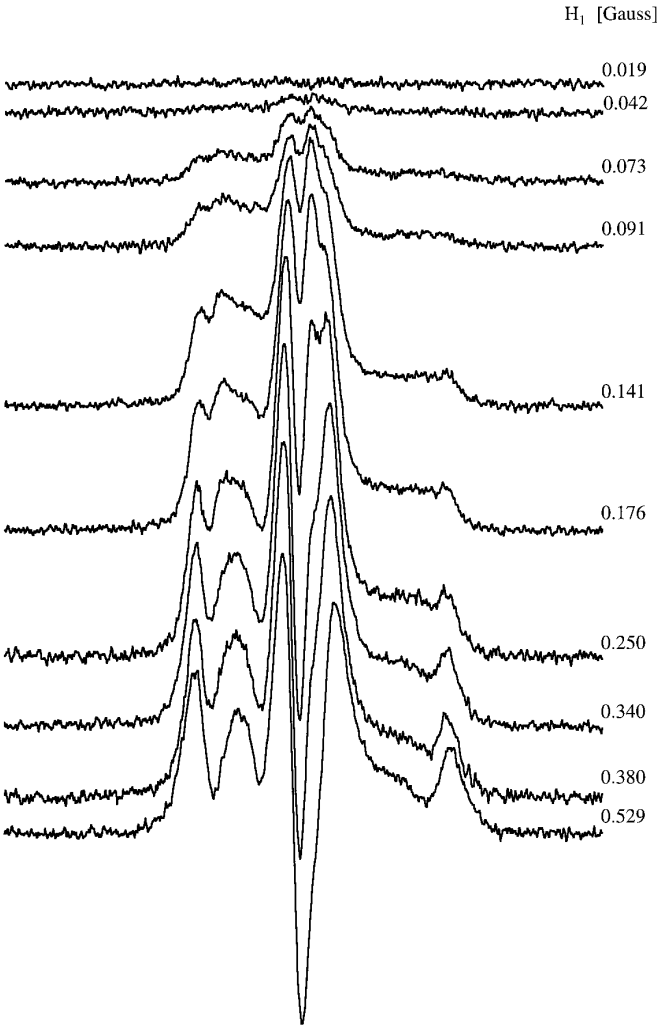

FIG. 2. Second-harmonic, 90° out-of-phase, absorption EPR spectra (V_2' display) of 0.22 mol% spin-labeled phosphatidylcholine (5-PCSL) in gel-phase dipalmitoyl phosphatidylcholine (DPPC) bilayer membranes at 15°C recorded at increasing (upper to lower) microwave magnetic field intensity, H_1. Modulation frequency $\omega_m/2\pi = 50$ kHz; modulation amplitude, $H_m = 5.0$ G; scan range = 160 G.

Larmor frequency. At low values of the radiation field H_1, the intensity of the out-of-phase signal is zero, corresponding to the absence of saturation. With increasing H_1, the central region of the spectrum first becomes positive and subsequently switches to becoming strongly negative at higher values of H_1. Experimental second-harmonic, out-of-phase absorption ST-EPR spectra at increasing microwave fields are given in Fig. 2 for a spin-labeled phospholipid at low concentration in gel-phase lipid bilayer membranes. The central hyperfine manifold in these anisotropic ^{14}N nitroxide powder spectra behaves qualitatively with increasing H_1 in a very similar manner to the simulated single-line spectra in Fig. 1.

The dependence of the integrated intensity of the experimental ST-EPR spectra of Fig. 2 on incident H_1 is given in Fig. 3. This characteristic saturation curve is similar in form to that obtained previously for spin-labeled hemoglobin (*17*). Integration over the entire lineshape removes the complications from the spectral anisotropy and inhomogeneous broadening and reveals the intrinsic saturation properties of the individual-component spin packets. Comparison is therefore possible with the saturation behavior of the normalized integral for a single spectral line. Simulated saturation curves for the integrated intensity of a single resonance line are given by the continuous lines in Fig. 3. It is clear from comparison of the upper and lower panels of the figure that variation of the T_1 and T_2 relaxation times has somewhat different effects on the saturation curves. However, unique values of T_1 and T_2 cannot be determined separately with precision by fitting the experimental saturation curve. The full lines in Fig. 3 represent the best fits that are obtained with a fixed value of T_2 and varying T_1. The value chosen for the transverse relaxation time is $T_2 = 20$ ns, which corresponds to the intrinsic Lorentzian linewidth obtained by Gaussian–Lorentzian deconvolution of the low-field line in the conventional V_1 EPR spectrum. A value of $T_1 = 2.9 \pm 0.4$ μs is obtained in this way by fitting the theoretically predicted saturation curves to the experimental data at this spin-label concentration (0.22 mol%). Estimation of the intrinsic value of the spin–lattice relaxation time of the spin label is significant, because this is the characteristic time scale to which the dynamic processes that give rise to relaxation enhancements are referred (*2, 3*).

Interestingly, the maximum intensity of the ST-EPR spectrum is obtained at a root-mean-square microwave field of $\langle H_1^2 \rangle^{1/2} = 0.25$ G, which is the same as that established in the standardized protocol for determining slow rotational diffusion rates by ST-EPR (*1*), although both the sample composition and the sample configuration are rather different in the present case.

T_1 dependence of ST-EPR intensities. The dependences of the normalized and unnormalized integrated intensities of the V_2' ST-EPR spectra on spin–lattice relaxation time, predicted from solution of the Bloch equations, are given in Fig. 4. Spectral simulations were made for various values of the spin–spin relaxation time, T_2, as indicated, and for the standard values of $H_1 = 0.25$ G and $H_m = 5.0$ G that are used experimentally in recording ST-EPR spectra (*11, 12*). Both normalized and unnormalized integrated intensities show similar dependences, but the former (I_{ST}) is preferred practically because it yields instrument-independent values (*13*).

The ST-EPR intensity shows a pronounced sensitivity to the spin–lattice relaxation rate for all but very short values

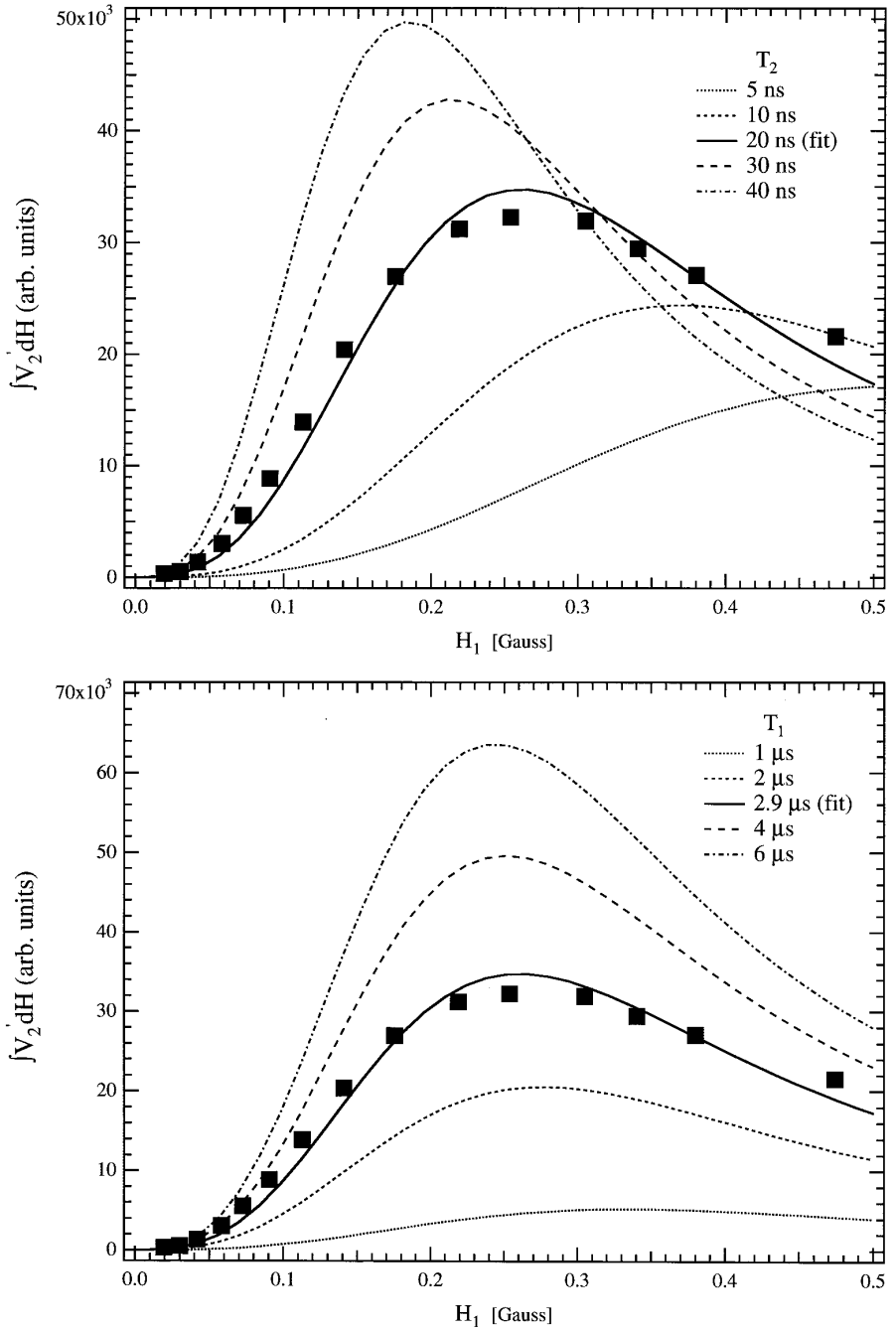

FIG. 3. Saturation curves for the first integral of the second-harmonic, 90° out-of-phase V_2' ST-EPR spectra with increasing microwave field, H_1. Filled squares are experimental points for 0.22 mol% 5-PCSL in DPPC bilayers at 15°C ($\omega_m/2\pi$ = 50 kHz; H_m = 5.0 G). (Upper panel) Lines are saturation curves deduced from spectra simulated with T_1 = 2.9 μs and the values of T_2 indicated (lower to upper: T_2 = 5 to 40 ns). (Lower panel) Lines are simulated curves for T_2 = 20 ns and the values of T_1 indicated (lower to upper: T_1 = 1–6 μs). The combination of T_1 = 2.9 ± 0.4 μs and T_2 = 20 ns represents a best fit of the simulated curves to the experimental data (see text).

of T_1. This dependence provides a theoretical basis for the experimental application of spin-label ST-EPR in determining spin–lattice relaxation enhancements (*2, 3*). Over an appreciable range, including that of practical interest in ST-EPR (*1*), the values of I_{ST} are approximately linearly related to T_1. The slope of the T_1 dependence does, however, depend somewhat on the value of T_2, although the form of the curves is relatively insensitive to T_2. This point is investigated fur-

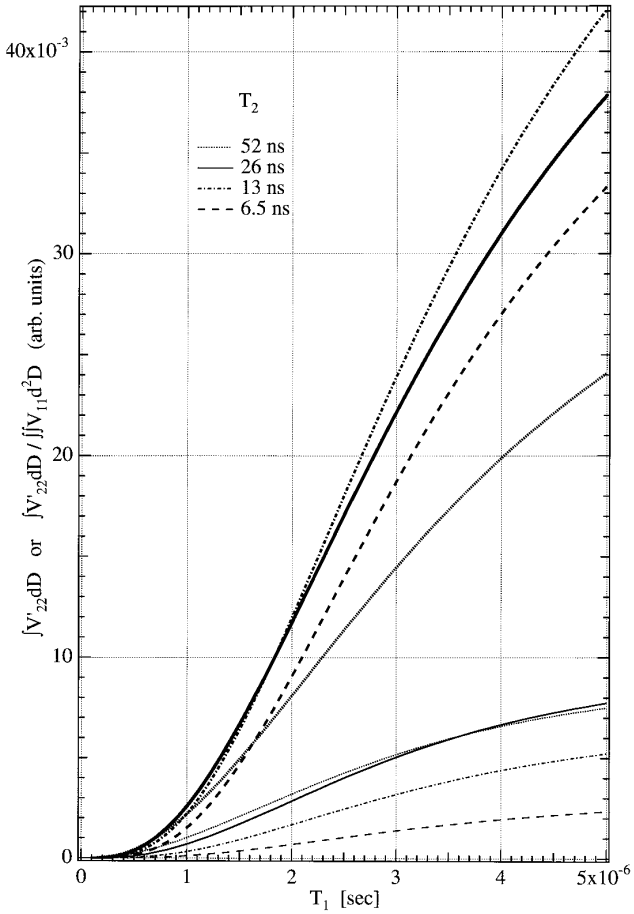

FIG. 4. Dependence of the integrated intensity of second-harmonic, 90° out-of-phase V_2' ST-EPR spectra on spin–lattice relaxation time, T_1, obtained from spectral simulation for the values of T_2 indicated (lower to upper: T_2 = 6.5–52 ns). Light curves are for the first integral of the V_2' ST-EPR spectra; heavy lines are the same quantity normalized to the second integral of the conventional V_1 EPR spectra ($\omega_m/2\pi$ = 50 kHz, H_1 = 0.25 G).

ther by measurements in which the effective spin–lattice relaxation rate is varied experimentally, either by Heisenberg exchange as a function of spin-label concentration or by paramagnetic relaxation as a function of Ni^{2+} ion concentration.

Correlation of ST-EPR intensity with conventional saturation measurements. The saturation parameters, or effective T_1T_2 values, have been varied by changing the concentration of the spin-labeled lipid in gel-phase bilayer membranes. The spin-label concentration was varied between 0.07 and 12 mol% to give varying degrees of alleviation of saturation by Heisenberg spin exchange (*4*). The correlation between the integrated intensities of the ST-EPR spectra and the saturation parameters (effective T_1T_2 products) determined from progressive-saturation measurements is given in Fig. 5. Data are given for two temperatures (15 and 25°C) in the $L_{\beta'}$ gel phase of DPPC bilayers and one temperature (35°C) in the intermediate $P_{\beta'}$ gel phase. The results at both temperatures in the $L_{\beta'}$ phase are comparable, but in the intermediate phase the values of the ST-EPR integral are smaller, and so are the corresponding values of the T_1T_2 product deduced from the progressive-saturation measurements. In all three cases, the ST-EPR intensity is related approximately linearly to the effective T_1T_2 product, as assumed previously from experimental results on relaxation enhancements by Heisenberg spin exchange (*4*) and by paramagnetic dipolar interactions (*9*). For the spin-label concentration range used, the effects of spin–spin interactions on T_1 dominate over those on T_2.

Fits to the theoretically predicted dependence of the ST-EPR intensity on T_1 are given by the full lines in Fig. 5. The optimum fits are obtained with a value of T_2 = 7–9 ns, which is considerably smaller than that deduced from the linewidths in the conventional V_1 EPR spectra (cf. above). The reason for this difference lies in the scaling of the T_1 dependence of the saturation parameter by the effective value of T_2 in the abscissa of Fig. 5. As noted previously in connection with Fig. 4, the form of the T_1 dependence is not sensitively dependent on the value of T_2. Low effective values

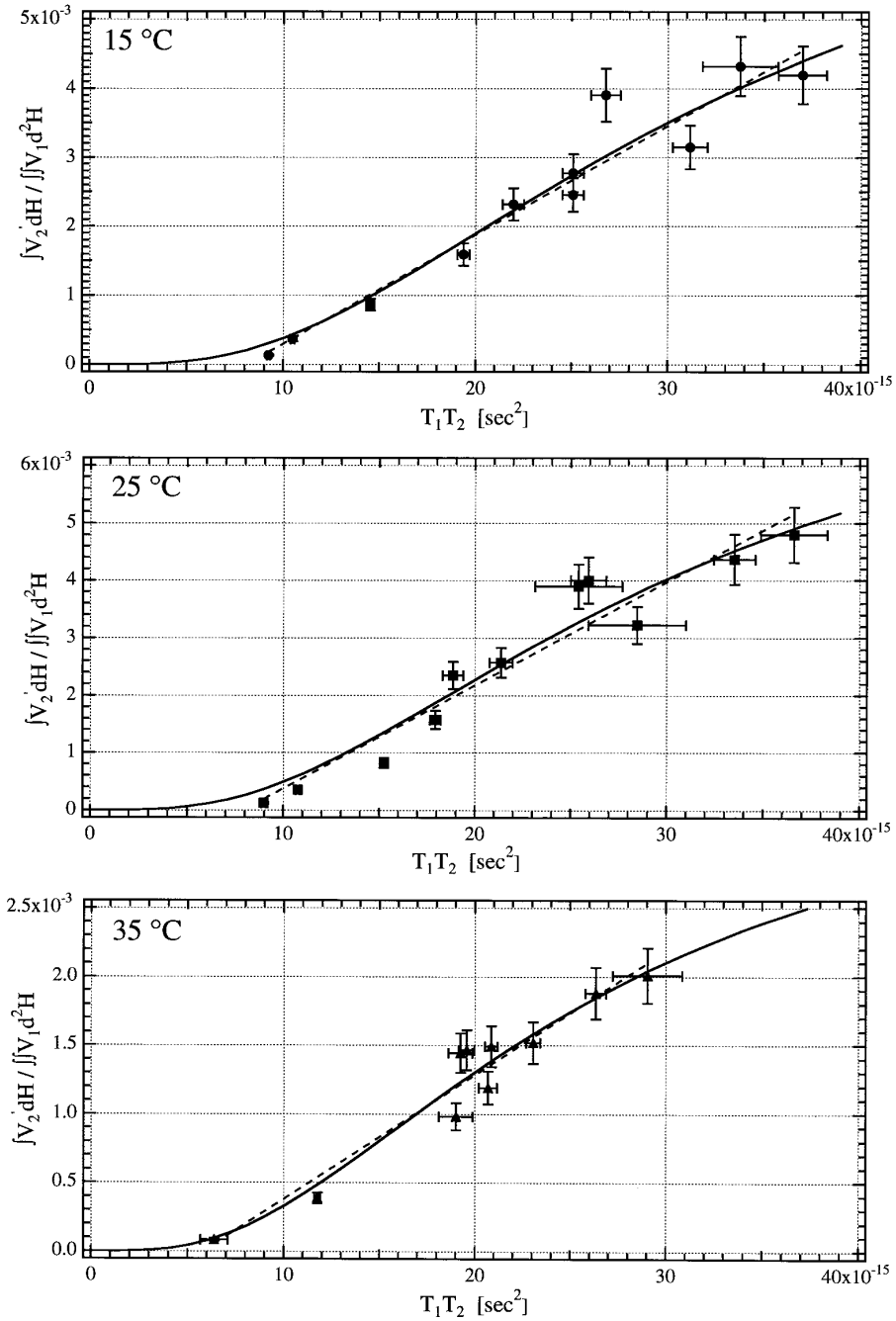

FIG. 5. Correlation of the integrated intensities of the V_2' ST-EPR spectra of the 5-PCSL spin-labeled lipid at different concentrations in gel-phase DPPC bilayers with the effective T_1T_2 relaxation time products obtained from progressive saturation of the second integral of the conventional V_1 EPR spectra. The V_2' spectra were recorded with $H_1 = 0.25$ G, $H_m = 5.0$ G, and $\omega_m/2\pi = 50$ kHz. Dashed lines are linear regressions, and full lines are fits to the theoretical dependence on T_1 (cf. Fig. 4). Upper, middle, and lower panels are data obtained at 15, 25, and 35°C, respectively. Effective values of $T_2 = 8.4 \pm 1.3$ ns (upper), 7.8 ± 1.1 ns (middle), and 6.6 ± 1 ns (lower) are obtained from the theoretical fits (full lines); see text.

of T_2 are required principally to bring the dependence of I_{ST} on the saturation parameter obtained from progressive saturation into the appropriate region of the predicted T_1 dependence. They do not appreciably affect the intrinsic dependence of I_{ST} on T_1. The effective values derived for T_2 are therefore best considered a (constant) scaling factor for the fits to the theoretical T_1 dependence. It should be noted that this effective value of T_2 gives rise to a value for

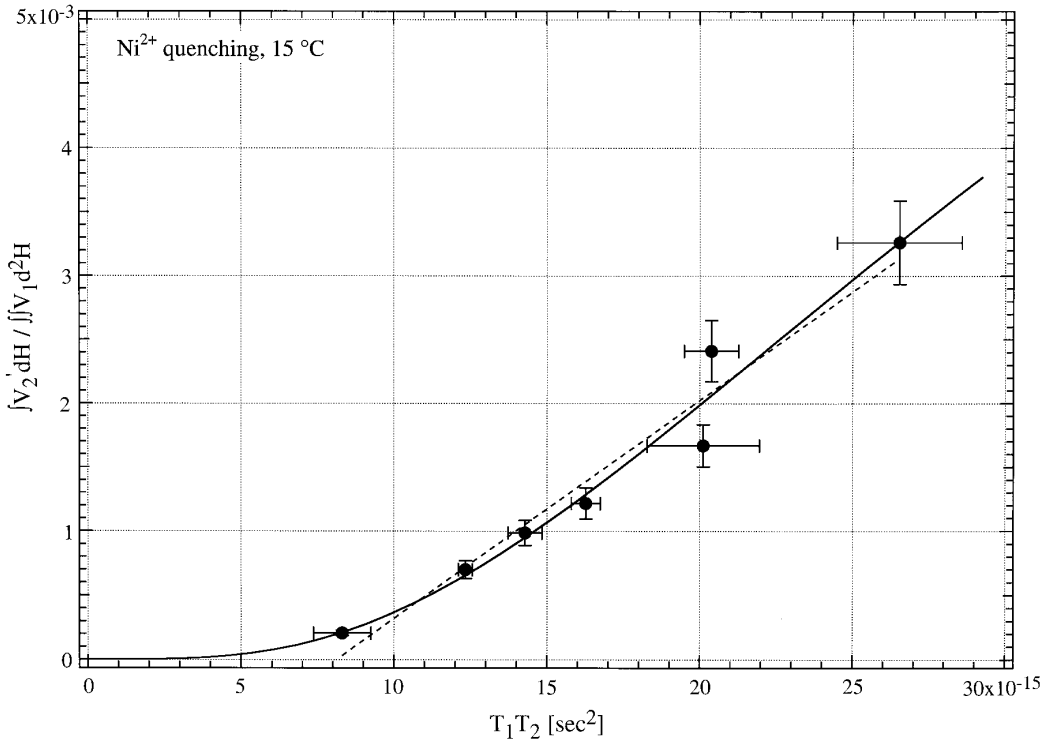

FIG. 6. Correlation of the integrated intensities of the V_2' ST-EPR spectra of the 5-PCSL spin-labeled lipid (0.5 mol%) in gel-phase DPPC at 15°C, in the presence of various concentrations of aqueous Ni^{2+}, with the effective T_1T_2 relaxation time products obtained from progressive saturation of the second integral of the conventional V_1 EPR spectra. The V_2' spectra were recorded with $H_1 = 0.25$ G, $H_m = 5.0$ G, and $\omega_m/2\pi = 50$ kHz. The dashed line is a linear regression and the full line is a fit to the theoretical dependence on T_1 (cf. Fig. 4), yielding an effective value of $T_2 = 9.4 \pm 1.7$ ns.

T_1 of 3 μs for the sample with 0.22 mol% spin label at 15°C, which is consistent with that obtained from fitting the ST-EPR saturation curve with the value of T_2 derived from the linewidth.

The saturation parameter (i.e., effective T_1T_2 product) has also been varied by addition of paramagnetic Ni^{2+} ions to the aqueous phase for gel-phase DPPC bilayers with a fixed concentration of the 5-PCSL spin label. The correlation between the values of I_{ST} obtained from the ST-EPR spectra and the effective T_1T_2 products determined from progressive-saturation measurements is given in Fig. 6. The dependence of I_{ST} on T_1T_2 with varying Ni^{2+} concentration is very similar to that obtained by varying the 5-PCSL spin-label concentration in gel-phase DPPC bilayers at 15°C, in the absence of Ni^{2+} (cf. Fig. 5, upper panel). Again, an approximately linear dependence is obtained and the regression parameters are, to within the error, identical to those obtained with varying spin-label concentration. Also, the fit of the theoretical dependence on T_1 to the experimental data is very similar and yields a comparable effective value of $T_2 = 9.4$ ns. Two quite independent means of varying the spin–lattice relaxation enhancement therefore yield completely consistent results for the dependence of the ST-EPR intensity on T_1.

The results given in Fig. 4, together with the fits of the data by simulation (Figs. 5 and 6), provide both a theoretical and an experimental basis for using the integrated intensities of V_2' ST-EPR spectra to determine effective spin–lattice relaxation enhancements of spin labels. Previous applications of this method were based primarily on empirical experimental correlations. Furthermore, the results allow a calibration of the ST-EPR intensities in terms of the effective relaxation times. From the linear regressions to the experimental data at both 15 and 25°C in the $L_{\beta'}$ phase, the following correlation is obtained,

$$I_{ST} \times 10^3 \approx 0.17 \times T_1(\mu s) T_2^{eff}(ns) - 1.3, \quad [19]$$

where an effective value of $T_2^{eff} \approx 8.5$ ns is appropriate to yield values of the spin–lattice relaxation time that are consistent with fits to the theoretical predictions. The rotational correlation times here are in the range $\tau_R \approx 20$–60 μs, and this calibration should be appropriate for systems in which rotational diffusion is very slow. The corresponding result obtained from the data at 35°C, in the intermediate gel phase, is

$$I_{ST} \times 10^3 \approx 0.09 \times T_1(\mu s) T_2^{eff}(ns) - 0.5, \quad [20]$$

where, in this case, an effective value of $T_2^{\text{eff}} \approx 6.6$ ns seems appropriate. This latter calibration corresponds to effective rotational correlation times in the region of $\tau_R \approx 2-40$ μs and may be applicable to systems undergoing somewhat faster rotational diffusion.

CONCLUSION

The dependence of the ST-EPR intensities on both microwave magnetic field intensity and effective relaxation times can be described by using the Bloch equations. This provides a theoretical basis for the use of ST-EPR intensities in determining spin–lattice relaxation enhancements. Such nonlinear CW measurements are more sensitive to changes in T_1 than are conventional progressive-saturation experiments (*4*) and are applicable to a range of biophysically relevant problems. Quantitatively, it is found that the effective spin–lattice relaxation times are likely to lie in the region of $T_1 = 3 \pm 1$ μs, depending on concentration, for spin labels in the systems of interest in ST-EPR experiments. This establishes the time scale for this type of measurement. Calibrations have been provided for the spin–lattice relaxation time in terms of the measured ST-EPR intensities in relevant cases. These should facilitate this alternative application of nonlinear spin-label EPR, particularly in studies on biological membranes.

ACKNOWLEDGMENTS

Partial support from the Hungarian National Science Foundation (F5506/1992 to T.P.) and the Russian Foundation for Basic Research (Grant 95-03-09604 to V.A.L.) is gratefully acknowledged.

REFERENCES

1. D. D. Thomas, L. R. Dalton, and J. S. Hyde, *J. Chem. Phys.* **65,** 3006–3024 (1976).
2. D. Marsh, *Chem. Soc. Rev.* **22,** 329–335 (1993).
3. D. Marsh, *Appl. Magn. Reson.* **3,** 53–65 (1992).
4. D. Marsh and L. I. Horváth, *J. Magn. Reson.* **97,** 13–26 (1992).
5. V. V. Khramtsov and D. Marsh, *Biochim. Biophys. Acta* **1068,** 257–260 (1991).
6. M. Esmann and D. Marsh, *Proc. Natl. Acad. Sci. USA* **89,** 7606–7609 (1992).
7. L. I. Horváth, P. J. Brophy, and D. Marsh, *Biophys. J.* **64,** 622–631 (1993).
8. T. Páli, R. Bartucci, L. I. Horváth, and D. Marsh, *Biophys. J.* **64,** 1781–1788 (1993).
9. T. Páli, R. Bartucci, L. I. Horváth, and D. Marsh, *Biophys. J.* **61,** 1595–1602 (1992).
10. D. Marsh and A. Watts, *in* ''Lipid–Protein Interactions'' (P. C. Jost and O. H. Griffith, Eds.), Vol. 2, pp. 53–126, Wiley–Interscience, New York, 1982.
11. P. Fajer and D. Marsh, *J. Magn. Reson.* **49,** 212–224 (1982).
12. M. A. Hemminga, P. A. de Jager, D. Marsh, and P. Fajer, *J. Magn. Reson.* **59,** 160–163 (1984).
13. L. I. Horváth and D. Marsh, *J. Magn. Reson.* **54,** 363–373 (1983).
14. T. Páli, L. I. Horváth, and D. Marsh, *J. Magn. Reson. A* **101,** 215–219 (1993).
15. K. Halbach, *Helv. Phys. Acta* **27,** 259–282 (1954).
16. D. D. Thomas and H. M. McConnell, *Chem. Phys. Lett.* **25,** 470–475 (1974).
17. T. C. Squier and D. D. Thomas, *Biophys. J.* **56,** 735–748 (1989).